Taylor & Francis
Taylor & Francis Group

Geomechanics and Geoengineering
An International Journal

ISSN: (Print) (Online) Journal homepage: www.tandfonline.com/journals/tgeo20

Two-phase interaction in isothermal hydro-mechanical-chemical coupling for improved carbon geological sequestration modelling

Sulaiman Abdullah, Yue Ma, Kai Wang, Shashank Subramanyam, Xiaohui Chen & Amirul Khan

To cite this article: Sulaiman Abdullah, Yue Ma, Kai Wang, Shashank Subramanyam, Xiaohui Chen & Amirul Khan (13 Dec 2023): Two-phase interaction in isothermal hydro-mechanical-chemical coupling for improved carbon geological sequestration modelling, Geomechanics and Geoengineering, DOI: 10.1080/17486025.2023.2292160

To link to this article: https://doi.org/10.1080/17486025.2023.2292160

Published online: 13 Dec 2023.

GEOMECHANICS AND GEOENGINEERING
https://doi.org/10.1080/17486025.2023.2292160

Taylor & Francis
Taylor & Francis Group

Two-phase interaction in isothermal hydro-mechanical-chemical coupling for improved carbon geological sequestration modelling

Sulaiman Abdullah, Yue Ma, Kai Wang, Shashank Subramanyam, Xiaohui Chen and Amirul Khan

Geomodelling and Artificial Intelligence Group, School of Civil Engineering, University of Leeds, Leeds, UK

ABSTRACT

Geological sequestration is an established method to store carbon deep underground. Many studies have proposed coupled constitutive models that can simulate such a complicated process; however, the coupling effect of multi-phase fluid flow and transport of chemical solutes in the liquid phase remains to be investigated. This study presents a multi-phase non-reactive hydro-mechanical-chemical constitutive framework under isothermal conditions based on mixture coupling theory. Non-equilibrium thermodynamics is used to generate an entropy production equation, and phenomenological equations use this to derive the chemical transport and interaction between two-phase fluid flows. This study proposes novel terms in the final governing equations. The model results are in good agreement with the results of a benchmark experiment and those found in the literature; the model has been used to compare the behaviour of carbon dioxide in the gas and supercritical phases. Sensitivity analysis was conducted to determine the effect of the parameters in the new terms. Sensitivity analysis revealed the significant impact of relative permeability and saturation values on the new terms, emphasising the importance of understanding frictional behaviour in porous media for accurate fluid flow modelling and prediction. This study urges further experimentation and model refinement to improve carbon sequestration modelling in larger formations.

ARTICLE HISTORY
Received 10 April 2023
Accepted 23 August 2023

KEYWORDS
Supercritical carbon dioxide; Non-equilibrium thermodynamics; Mixture coupling theory; Two-Phase fluid transport; Carbon sequestration; Two-phase interaction

1. Introduction

Recent research has included novel studies on a fully coupled multi-phase hydro-mechanical-supercritical-chemical phase transport model for carbon sequestration applications (André *et al.* 2007, Sasaki *et al.* 2008, Alonso *et al.* 2012, Nasvi *et al.* 2013, Yamamoto *et al.* 2013, Bao *et al.* 2014, LI and Laloui 2016a, Zhang *et al.* 2016, Islam *et al.* 2020, Lu and Zhang 2020). These efforts aim to advance our understanding and application of carbon capture techniques, contributing significantly to efforts to mitigate our carbon footprint. Additionally, certain researchers are exploring how to leverage the carbon sequestration process not just for environmental remediation, but also as a means to enhance hydrocarbon production such as methane (Fan et al. 2019, 2023). Within the broader context of subsurface processes, recent studies have also shed light on coal–water interactions and their influence on gas extraction from coal, as well as on the multi-physics coupling involved in coal and gas outbursts (Liu et al. 2021, 2021). The carbon sequestration process usually requires multi-phase flow modelling because the storing process is often conducted in aquifers or formations that contain other fluids, such as oil and natural gas. Early research, such as Meiri (1981) and Schrefler and Xiaoyong (1993), attempted to develop a general two-phase hydro-mechanical (HM) model to describe the transport of fluids (such as water) and air in deformable porous media. Whereas Meiri (1981) used a basic model to simulate a 1D air storage case, the Schrefler and Xiaoyong (1993) model was more advanced and had better validation against known cases, such as Liakopoulos (1965b). However, the mechanical governing equations are relatively simple, and the model lacks the ability to simulate the effect of chemical solute transport and two-phase interaction energy dissipation on the total energy of the system. Later, Li and Laloui (2016b) proposed a coupled multi-phase modelling framework for the carbon sequestration process in the supercritical phase. The presented thermo-hydro-mechanical model (THM) simulated the supercritical CO_2 ($ScCO_2$) injection process. The main innovation of the model was thermal coupling, in which the Joule-Thomas effect was incorporated into the THM model. Although the presented model appears to have a good thermal coupling capability, it is a more simplified version with just mechanical coupling, and the transport of chemical solutes being ignored. Moreover, the

CONTACT Xiaohui Chen x.chen@leeds.ac.uk

dissipation energy due to the two-phase interaction fluids remained uninvestigated. Due to the complexity of chemical coupling transport in the multi-phase, many researchers prefer to use simulators such as TOUGHREACT or AD-GPRS/GFLASH to simulate the $ScCO_2$ sequestration process when chemical transport and reactions are considered (Xu et al. 2003, 2010, André *et al.* 2007, Taron and Elsworth 2009, Xiao *et al.* 2009, Liu *et al.* 2011, Zhang et al. 2012, 2015, 2016, Wolf *et al.* 2016, Siqueira *et al.* 2017, Voskov *et al.* 2017). The simulators have acceptable results; however, the scope of this research is to focus on the mathematical derivation and governing equations rather than simulations. Islam *et al.* (2020) presented a two-phase coupled model for a CO_2 sequestration project to investigate the possibility of fluid leakage. The authors derived a general form of the coupled equations and obtained two schemes: the capillary and gas pressure scheme and the liquid pressure and gas saturation scheme. This method attempts to simplify the solution of the numerical simulation while retaining the coupled HM interaction. The model is then compared to others in the literature, such as those developed in Refs (Richards 1931, Liakopoulos 1965b, Kueper and Frind 1991, Schrefler and Xiaoyong 1993); however, the model neglected the chemical solute transport and friction results from the interaction between solid/gas-Sc, solid/liquid, and liquid/gas-Sc flows.

The effects of transported solutes and the friction dissipation energy on some parameters such as pressure, deformation, saturation and other properties due to the multi-flow of $ScCO_2$ and formation liquid have yet to be fully explored. This study investigates the effect of solute transport within a liquid on fluid energy and the effect of friction between each phase. A mathematical model is developed using the mixture coupling theory approach. Mixture coupling theory is an energy approach which was developed by Heidug and Wong (1996). Since then, the model has been known by modified mixture theory or mixture coupling theory (Chen 2010, Chen and Hicks 2011, Chen *et al.* 2016, Ma *et al.* 2020, Abdullah *et al.* 2022). The mixture coupling theory is a modification of the mixture theory by viewing a fluid-infiltrated rock/soil as a single continuum instead of explicitly discriminating between the solid and fluid phases (Heidug and Wong 1996). Moreover, it overcomes the challenges in mixture theory and shows advantages over the classic mechanics approach (Coussy *et al.* 1998). Additionally, unlike the classical mechanics approach, which uses the stress-strain tensor and balance of linear momentum, the mixture coupling theory is based on non-equilibrium thermodynamics and uses energy and entropy analysis. The difference between the two methods is discussed in more detail in Refs (Chen and Hicks 2011, Abdullah *et al.* 2022). The mixture coupling theory, in contrast to some other energy approaches that also utilise non-equilibrium thermodynamics, omits the momentum conservation balance equation. The objective of this research is not to delve into the differences between the mixture coupling theory and other methods. To do so, readers are directed to Siddiqui *et al.* (2023), who discussed the THCM continuum modelling, emphasising thermodynamics-based constitutive models in depth.

The remainder of this paper is organised as follows: Section 2 introduces a model for the transport of two-phase fluids in a deformable porous medium, before Sec. 3 models the dissipation entropy of the system. Section 4 describes the coupling of the models in Secs. 2 and 3 and develops the phenomenological equations of the system. Section 5 determines the constitutive equations, and Sec. 6 validates the model against numerical simulations. The study and its contributions are listed in Sec. 7.

2. Physical model

This model considers the transport of two-phase fluids, $ScCO_2$ and saline water flows, in a deformable porous medium under isothermal conditions. The couplings between the fluids and deformation are considered. Since saline water consists of water and a chemical (NaCl), the chemical transport modulus is also studied. To simplify the discussion, the following are assumed: (I) chemical reactions, either between/within the fluids or between fluid-solid, are not considered; (II) the chemical solute/minerals only exist in the liquid phase (saline water); (III) carbon dioxide in the supercritical phase is chemically non-reactive; (IV) the system is immiscible, in which the mass does not exchange between the liquid and supercritical phases through dissolution; (V) the process is under isothermal conditions; and (VI) the porous media has a completely isotropic behaviour (isotropic material).

To develop the constitutive model, an arbitrary microscopic domain which is large enough to include all phases, with surface boundary Γ enclosing the domain V, is selected. Only fluids are allowed to pass through the boundary.

Let the superscript Sc represent $ScCO_2$ and l represent saline water; the volume of the two flows are V^{Sc} and V^{l}, respectively. If the volume of the pore space is V^{pore}, the following relationship can be obtained:

$$V^{pore} = V^{Sc} + V^{l},\ \phi = \phi^{Sc} + \phi^{l},\ S^{Sc} + S^{l} = 1, \quad (1)$$

where $\phi = V^{pore}/V$, $\phi^{Sc} = V^{Sc}/V$, and $\phi^{l} = V^{l}/V$ are the volume fractions (porosity) of the pore space, $ScCO_2$, and saline water, respectively; $S^{Sc} = V^{Sc}/V^{pore}$ is the saturation of the $ScCO_2$; and $S^{l} = V^{l}/V^{pore}$ is the saturation of the saline water.

The mixture density (mass divided by total mixture volume) can be linked to the phase density (mass divided by phase volume) using

$$\rho^{l} = \phi^{l}\rho_{l}^{l},\ \rho^{Sc} = \phi^{Sc}\rho_{Sc}^{Sc} \quad (2)$$

where ρ^{l} and ρ^{Sc} are the mixture densities and ρ_{l}^{l} and ρ_{Sc}^{Sc} are the phase densities.

Any constituent in one phase follows a similar density relationship. For example, for the chemical c and water w in the saline water, the following holds:

$$\rho^{w} = \phi^{l}\rho_{l}^{w}, \rho_{l}^{c}\ and\ \rho^{l} = \rho^{w} + \rho^{c} \quad (3)$$

where ρ_{l}^{w} is the mass of the water divided by the total liquid (phase) volume and ρ_{l}^{c} is the mass of the chemical divided by the total liquid (phase) volume.

2.1. Flux equations

Let β represent either the saline water flow l or supercritical $ScCO_2$ flow Sc, as well as the sub-constituents of saline water, such as water and chemical; the mass flux of β is defined as

$$\mathbf{I}^{\beta} = \rho^{\beta}\left(\mathbf{v}^{\beta} - \mathbf{v}^{s}\right), \quad (4)$$

where ρ^{β} is the mixture density of β, $\mathbf{v}^{\beta}$ is the velocity of β, and $\mathbf{v}^{s}$is the velocity of the solid.

The diffusion flux $\mathbf{J}^{\beta}$ of β, relative to the barycentric velocity, can be expressed as:

$$\mathbf{J}^{\beta} = \rho^{\beta}\left(\mathbf{v}^{\beta} - \mathbf{v}^{l}\right)\beta \in l \quad (5)$$

$$\mathbf{J}^{\beta} = \rho^{\beta}\left(\mathbf{v}^{\beta} - \mathbf{v}^{Sc}\right)\beta \in Sc \quad (6)$$

where $\mathbf{v}^{l} = \frac{\rho^{w}}{\rho^{l}}\mathbf{v}^{w} + \frac{\rho^{c}}{\rho^{l}}\mathbf{v}^{c}$ is the barycentric velocity of saline water.

In Equation (6), because we regarded the $ScCO_2$ flow to be composed of a single constituent, $\mathbf{v}^{\beta} = \mathbf{v}^{Sc}$, which means that the diffusion flux of the $ScCO_2$ flow is zero. However, in Equation (5), saline water flow contains water and a chemical; therefore, $\mathbf{v}^{w} \neq \mathbf{v}^{l}$ and $\mathbf{v}^{c} \neq \mathbf{v}^{l}$.

Considering the flux Equation (4), the diffusion flux (5) can be written as

$$\mathbf{J}^{\beta} = \mathbf{I}^{\beta} - \rho^{\beta}\left(\mathbf{v}^{l} - \mathbf{v}^{s}\right). \quad (7)$$

2.2. Mass and energy balance equations

2.2.1. Helmholtz free energy

The Helmholtz free energy balance equation for the considered mixture system (Heidug and Wong 1996) can be written as (Heidug and Wong 1996):

$$\frac{D}{Dt}\left(\int_{V}\psi dV\right) = \int_{\Gamma}\boldsymbol{\sigma}\mathbf{v}^{s}\cdot\mathbf{n}d\Gamma - \left(\int_{\Gamma}\mu^{w}\mathbf{I}^{w} + \int_{\Gamma}\mu^{Sc}\mathbf{I}^{Sc} + \int_{\Gamma}\mu^{c}\mathbf{I}^{c}\right)\cdot\mathbf{n}d\Gamma - T\int_{V}\gamma dV \quad (8)$$

where ψ is the Helmholtz free energy density; $\boldsymbol{\sigma}$ is the Cauchy stress tensor; $\mathbf{n}$ is the outward unit normal vector; μ^{w}, μ^{Sc}, and μ^{c} are chemical potentials of the water, $ScCO_2$, and chemical (NaCl), respectively; T. is the constant temperature and γ is the entropy production per unit volume.

The material time derivative following motion of the solid is $\frac{d(\cdot)}{dt} = \frac{\partial(\cdot)}{\partial t} + \mathbf{v}^{s}\cdot\quad(\cdot)$; then, the differential form of the balance equation of the free energy density can be written as:

$$\dot{\psi} + \psi\quad\cdot\mathbf{v}^{\mathbf{s}} - \quad\cdot(\boldsymbol{\sigma}\mathbf{v}^{\mathbf{s}}) + \quad\cdot\left(\mu^{w}\mathbf{I}^{w} + \mu^{Sc}\mathbf{I}^{Sc} + \mu^{c}\mathbf{I}^{c}\right) = -T\gamma \leq 0. \quad (9)$$

2.2.2. Fluid balance equation

Because no reactions are considered, the change of mass is only through the flux; therefore, the balance equation for the fluid can be expressed as (Chen 2013, Chen *et al.* 2018):

$$\frac{D}{Dt}\left(\ {}_{V}\ \rho^{\beta}dV\right) = -\ {}_{\Gamma}\ \mathbf{I}^{\beta}\cdot\mathbf{n}d\Gamma, \quad (10)$$

and the local form is:

$$\dot{\rho}^{\beta} + \rho^{\beta}\quad\cdot\mathbf{v}^{s} + \quad\cdot\mathbf{I}^{\beta} = 0. \quad (11)$$

3. Dissipation entropy

The entropy product results from dissipative processes, such as the friction generated at the solid/fluid phase boundary when fluid moves through a solid matrix. Moreover, the transport of the solute (chemical transport) has a dissipation effect. The entropy product can be divided into three parts: entropy induced by the saline water fraction, entropy induced by the supercritical fraction, and entropy by chemical transport. Using non-equilibrium thermodynamics, entropy production is described by Katachalsky and Curran (1965) as:

$$0 \le T\gamma = -\mathbf{I}^{w} \cdot \quad \mu^{w} - \mathbf{I}^{Sc} \cdot \quad \mu^{Sc} - \mathbf{I}^{c} \cdot \quad \mu^{c}. \tag{12}$$

The Darcy velocity **u** applies to both the liquid (including the chemicals/solute) and supercritical and can be written as

$$\mathbf{u}^{l} = S^{l}\phi\left(\mathbf{v}^{l} - \mathbf{v}^{s}\right), \mathbf{u}^{Sc} = S^{Sc}\phi\left(\mathbf{v}^{Sc} - \mathbf{v}^{s}\right). \tag{13}$$

Using the relationship in Equation. (7) and (13), as well as substituting the density relationship (2) into Equation (12), the following is obtained.

$$0 \le T\gamma = -\mathbf{u}^{l} \cdot \quad p^{l} - \mathbf{J}^{c} \cdot \quad (\mu^{c} - \mu^{w}) - \mathbf{u}^{Sc} \cdot \quad p^{Sc}, \tag{14}$$

in which $-\mathbf{u}^{l} \cdot \quad p^{l}$ represents the liquid Darcy velocity driven by liquid pressure p^{l}, $\mathbf{J}^{c} \cdot \quad (\mu^{c} - \mu^{w})$ represents the chemical diffusion in the liquid water driven by chemical potentials, and $-\mathbf{u}^{Sc} \cdot \quad p^{Sc}$ represents the supercritical Darcy velocity driven by supercritical pressure.

Equation (14) describes the entropy production with the driving forces of each flow. To describe the interaction between flows and driving forces as a linear relationship, the concept of the phenomenological equation may be used (Chen *et al.* 2018).

4. Coupled phases interactions and phenomenological equations

As each flux may influence another flux (coupled), the interaction between flows and driving forces can be expressed as the linear dependence of the three flows on their corresponding force equations (phenomenological equations). The three flows $\rho_{t}^{l}\mathbf{u}^{l}, \rho_{t}^{Sc}\mathbf{u}^{Sc}$,and $\mathbf{J}^{c}$, and the three major driving forces p^{l}, p^{Sc}, and $(\mu^{c} - \mu^{w})$ can be calculated using mass transport in isotropic media (Karrech 2013, Chen *et al.* 2018):

$$\rho_{l}^{l}\mathbf{u}^{l} = -\frac{L_{11}}{\rho_{l}^{l}} \quad p^{l} - \frac{L_{12}}{\rho_{Sc}^{Sc}} \quad p^{Sc} - L_{13} \quad (\mu^{c} - \mu^{w}), \tag{15}$$

$$\rho_{t}^{Sc}\mathbf{u}^{Sc} = -\frac{L_{21}}{\rho_{l}^{l}} \quad p^{l} - \frac{L_{22}}{\rho_{Sc}^{Sc}} \quad p^{Sc} - L_{23} \quad (\mu^{c} - \mu^{w}), \tag{16}$$

$$\mathbf{J}^{c} = -\frac{L_{31}}{\rho_{l}^{l}} \quad p^{l} - \frac{L_{32}}{\rho_{Sc}^{Sc}} \quad p^{Sc} - L_{33} \quad (\mu^{c} - \mu^{w}), \tag{17}$$

where L_{ij} are phenomenological coefficients.

Equations (15)-(17) describe the coupled fluid flows (liquid water/$ScCO_2$) and diffusion flux in the liquid phase (NaCl/liquid water) with the coupled influence of liquid and supercritical pressures and chemical potential difference.

Since the use of chemical potentials is uncommon in geomechanics, it is replaced with chemical concentration c^{α}. Using non-equilibrium thermodynamics, the difference in chemical potential can be written as (Chen *et al.* 2018):

$$\mathbf{u}^{l} = -k_{abs}\frac{k_{rl}}{\nu^{w}}\left(\quad p^{l} - r_{1}\frac{\rho_{l}^{l}}{\rho_{Sc}^{Sc}} \quad p^{Sc} - r_{2}\rho_{l}^{l}\left(\frac{1}{c^{w}}\frac{\partial\mu^{c}}{\partial c^{c}} \quad c^{c}\right)\right), \tag{18}$$

$$\mathbf{u}^{Sc} = -k_{abs}\frac{k_{rSc}}{\nu^{Sc}}\left(-r_{3}\frac{\rho_{Sc}^{Sc}}{\rho_{l}^{l}} \quad p^{l} + \quad p^{Sc} - \rho_{Sc}^{Sc}r_{4}\left(\frac{1}{c^{w}}\frac{\partial\mu^{c}}{\partial c^{c}} \quad c^{c}\right)\right), \tag{19}$$

$$\mathbf{J}^{c} = -\left(\frac{L^{l}\rho_{l}^{l}}{p^{l}}\right) \quad p^{l} - \left(\frac{L^{Sc}\rho_{Sc}^{Sc}}{p^{Sc}}\right) \quad p^{Sc} - D\rho^{l} \quad c^{c}, \tag{20}$$

coefficients can be defined as:

$$k_{abs}\frac{k_{rl}}{\nu^{w}} = \frac{L_{11}}{\left(\rho_{l}^{l}\right)^{2}}, r_{1} = -\frac{L_{12}}{L_{11}}, r_{2} = -\frac{L_{13}}{L_{11}}, r_{3} = -\frac{L_{21}}{L_{22}},$$

$$r_{4} = -\frac{L_{23}}{L_{22}}L^{l} = -\frac{L_{31}p^{l}}{\left(\rho_{l}^{l}\right)^{2}}, L^{Sc} = -\frac{L_{32}p^{Sc}}{\left(\rho_{Sc}^{Sc}\right)^{2}}, D = \frac{L_{33}}{c^{w}\rho_{l}^{l}}\frac{\partial\mu^{c}}{\partial c^{c}}$$

where k_{abs} are the absolute (intrinsic) permeabilities, k_{rl} and k_{rSc} are the relative permeabilities, ν^{w} and ν^{Sc} are the viscosities, and p^{l} and p^{Sc} are the pore pressures, each for saline water and $ScCO_2$, respectively. c^{w} and c^{c} are the mass fraction of water and chemical solute (NaCl), respectively. Parameters r_1 and r_3 relate to the two-phase friction/dissipation and r_2 and r_4 relate to the chemical transport energy dissipation.

Equation (18) contains the three coupling terms that affect the Darcy velocity of the liquid phase (saline water): p^{l} represents the main driving force, which is the pressure gradient of the liquid; $r_{1}\frac{\rho_{l}^{l}}{\rho_{Sc}^{Sc}} \quad p^{Sc}$ represents the effect of the supercritical-phase friction/dissipation on the Darcy velocity of the liquid and $\rho_{Sc}^{Sc}r_{4}\left(\frac{1}{c^{w}}\frac{\partial\mu^{c}}{\partial c^{c}} \quad c^{c}\right)$ represents the coupling effect between the supercritical-phase and solute. The same terms apply to Equation (19) for the second-phase flow (supercritical).

The terms mentioned above represent the key findings of this study. The effects of these coupling terms will be discussed in the subsequent section, where they are incorporated into the governing equations. Utilising these phenomenological relations enables this approach to capture the impact of each flow on the others, specifically in terms of friction.

5. Constitutive equations

The solid/rock is assumed to be in mechanical equilibrium (e.g. $\cdot\,\boldsymbol{\sigma} = 0$). Using the entropy product in

Equation (12) and the free energy Equation (9), the equation for the Helmholtz free energy density ψcan be written as

$$\dot{\psi} + \psi \quad \cdot \mathbf{v}^s - (\boldsymbol{\sigma} : \quad \mathbf{v}^s) + \mu^w \quad \cdot \mathbf{I}^w + \mu^{Sc} \quad \cdot \mathbf{I}^{Sc} + \mu^c \quad \cdot \mathbf{I}^c = 0. \tag{21}$$

To use classic continuum mechanics to determine the rock deformation, several basic relationships are required. For an arbitrary reference configuration $\mathbf{X}$ at time t and position $\mathbf{x}$, the deformation gradient $\mathbf{F}$ and Green strain $\mathbf{E}$ can be expressed as (Wriggers 2008):

$$\mathbf{F} = \frac{\partial \mathbf{x}}{\partial \mathbf{X}}(\mathbf{X}, t),\ \mathbf{E} = \frac{1}{2}\left(\mathbf{F}^{\mathrm{T}}\mathbf{F} - \mathbf{I}\right), \tag{22}$$

where $\mathbf{I}$ is a unit tensor. The second Piola-Kirchhoff stress tensor $\mathbf{T}$ is introduced to measure stress in the reference configuration; the relationship between $\mathbf{T}$ and $\boldsymbol{\sigma}$ is:

$$\mathbf{T} = J\mathbf{F}^{-1}\boldsymbol{\sigma}\mathbf{F}^{-T}, \tag{23}$$

where J is the Jacobian of $\mathbf{F}$, expressed as:

$$J = \frac{dV}{dV_0},\ \dot{J} = J \quad \mathbf{v}^s, \tag{24}$$

where dV and dV_0 are the volumes of the current and reference configurations, respectively.

The following holds at the reference configuration:

$$\Psi = J\psi,\ m^\beta = J\rho^\beta = JS^\beta\phi\rho_\beta^\beta, \tag{25}$$

where Ψ is the free energy in the reference configuration and m^β is the mass density of the three flows in the reference configuration. Then, using Equation. (11) and (21) with Equation. (22)-(25), the differential form of the free energy in the reference configuration can be written as:

$$\dot{\Psi} = tr\left(\mathbf{T}\dot{\mathbf{E}}\right) + \mu^w\dot{m}^w + \mu^{Sc}\dot{m}^{Sc} + \mu^c\dot{m}^c. \tag{26}$$

5.1. Helmholtz free energy density of pore space

The Helmholtz free energy density of the pore, which contains saline water and CO_2 in the supercritical phase, is denoted as ψ^{pore}. From classical thermodynamics,

$$\psi^{pore} = -p^p + S^l\left(\mu^w\rho_l^w + \mu^c\rho_l^c\right) + S^{Sc}\mu^{Sc}\rho_{Sc}^{Sc}, \tag{27}$$

where p^p is the average pressure in the pore space.

The derivative form can be written as:

$$\dot{\psi}^{\mathrm{pore}} = \mu^w\left(S^l\rho_l^w\right) + \mu^c\left(S^l\rho_l^c\right) + \mu^{Sc}\left(S^{Sc}\rho_{Sc}^{Sc}\right). \tag{28}$$

5.2. Free energy density of solid matrix

The free energy density stored in the solid matrix can be calculated by subtracting the free energy of the pore liquid/supercritical $J\phi\psi^{pore}$ from the total free energy of the combined rock/liquid/supercritical system Ψ (e.g. $\Psi - J\phi\psi^{pore}$). $v = J\phi$ is the pore volume fraction in the reference configuration. Using Equations (26) and (28), the free energy of the wetted mineral matrix is obtained as:

$$\left(\Psi - J\phi\psi^{pore}\right)^{\cdot} = tr\left(\mathbf{T}\dot{\mathbf{E}}\right) + p^p\dot{v}. \tag{29}$$

The dual potential can be expressed as

$$W = \left(\Psi - J\phi^w\psi_{\mathrm{pore}}\right) - p^p v. \tag{30}$$

Substituting Equation (29) into the time derivative of Equation (30) yields

$$\dot{W}(\mathbf{E}, p^p) = tr\left(\mathbf{T}\dot{\mathbf{E}}\right) - \dot{p}^p v, \tag{31}$$

where $W$is a function of $\mathbf{E}$ and p^p; therefore, it can be written as

$$\dot{W}(\mathbf{E}, p^p) = \left(\frac{\partial W}{\partial E_{ij}}\right)_{p^p}\dot{E}_{ij} + \left(\frac{\partial W}{\partial p^p}\right)_{E_{ij}}\dot{p}^p \tag{32}$$

and

$$T_{ij} = \left(\frac{\partial W}{\partial E_{ij}}\right)_{p^p}, v = -\left(\frac{\partial W}{\partial p^p}\right)_{E_{ij}}, \tag{33}$$

$$\dot{T}_{ij} = L_{ijkl}\dot{E}_{kl} - M_{ij}\dot{p}^p, \tag{34}$$

$$\dot{v} = M_{ij}\dot{E}_{ij} + Q\dot{p}^p, \tag{35}$$

where the parameters L_{ijkl}, M_{ij}, and Q can be described as

$$\begin{aligned} L_{ijkl} &= \left(\frac{\partial T_{ij}}{\partial E_{kl}}\right)_{p^p} = \left(\frac{\partial T_{kl}}{\partial E_{ij}}\right)_{p^p} \\ M_{ij} &= -\left(\frac{\partial T_{ij}}{\partial p^p}\right)_{E_{ij}} = \left(\frac{\partial v}{\partial E_{ij}}\right)_{p^p} \\ Q &= \left(\frac{\partial v}{\partial p^p}\right)_{E_{ij},\mu^b} \end{aligned}. \tag{36}$$

by using the porosity definition in Equation. (11):

$$\frac{\partial\left(\phi^\beta\rho_\beta^\beta\right)}{\partial t} + \left(\phi^\beta\rho_\beta^\beta\right) \quad \cdot \mathbf{v}^\beta + \quad \cdot \mathbf{I}^\beta = 0. \tag{37}$$

by using mixture density Equations (2) and (37), then substituting into equation (7), it leads to:

$$S^l v\rho_l^l\frac{\partial c^\beta}{\partial t} + \rho_l^l\mathbf{u}^l \cdot \quad c^\beta + \quad \cdot \mathbf{J}^\beta = 0. \tag{38}$$

5.3. Governing field equations

5.3.1. Mechanical behaviour

To simplify the discussion of the mechanical phase, three assumptions are made:

(i) The mechanical behaviour is regarded as a small strain condition; therefore, the Green strain tensor E_{ij} and Piola-Kirchhoff stress T_{ij} can be replaced by strain tensor ε_{ij} and Cauchy stress $\boldsymbol{\sigma}_{ij}$, respectively.

$$E_{ij} \approx \varepsilon_{ij} \quad , T_{ij} \approx \boldsymbol{\sigma}_{ij} \tag{39}$$

(ii) For mechanical equilibrium, it can be assumed that $\frac{\partial \boldsymbol{\sigma}_{ij}}{\partial x_j} = 0$. Additionally, L_{ijkl}, M_{ij}, and Q are assumed to be material-dependent constants. Moreover, the material is assumed to be fully isotropic, in which M_{ij} is diagonal and can be expressed as:

$$M_{ij} = \zeta \delta_{ij}, \tag{40}$$

where ζ is Biot's coefficient.

(iii) The porous medium is assumed to exhibit completely isotropic behaviour; it is an isotropic material

The elastic stiffness L_{ijkl} can be written as a fourth-order isotropic tensor:

$$L_{ijkl} = G\left(\delta_{ik}\delta_{jl} + \delta_{il}\delta_{jk}\right) + \left(K - \frac{2G}{3}\right)\delta_{ij}\delta_{kl}, \tag{41}$$

where G and K are the rock shear and bulk moduli, respectively.

The governing stress Equation (34) can be written as

$$\dot{\boldsymbol{\sigma}}_{ij} = \left(K - \frac{2G}{3}\right)\dot{\varepsilon}_{kk}\delta_{ij} + 2G\dot{\varepsilon}_{ij} - \zeta \dot{p}^p \delta_{ij}. \tag{42}$$

The porosity change is related to the strain and pore fluid pressure by

$$\dot{v} = \zeta \dot{\varepsilon}_{ii} + Q\dot{p}^p. \tag{43}$$

From Heidug and Wong (1996), Q and ζ can be expressed as:

$$Q = \frac{\zeta - \phi}{K^s}, \tag{44}$$

$$\zeta = 1 - \frac{K}{K^s}. \tag{45}$$

The mechanical governing equation can be expressed as:

$$G \ {}^2\dot{\mathbf{d}} + \left(\frac{G}{1-2\theta}\right) \ (\ \cdot \dot{\mathbf{d}}) - \zeta \ \dot{p}^p = 0. \tag{46}$$

where $\mathbf{d}$ is displacement and θ is Poisson's ratio. The average pore pressure in the pore space can be expressed as (Lewis and Schrefler 1987)

$$p^p = p^l S^l + p^{Sc} S^{Sc} = p^l S^l + p^{Sc} - S^l p^{Sc}. \tag{47}$$

Then, by using Eq. (47), Eq. (46) can be expanded to the final governing equation for the mechanical behaviour:

$$G \ {}^2\dot{\mathbf{d}} + \left(\frac{G}{1-2\theta}\right) \ \left(\ \cdot \dot{\mathbf{d}}\right) - \zeta \ \left[\left(S^l + c^s p^c\right)\dot{p}^l\right] - \zeta \ \left[\left(S^{Sc} - c^s p^c\right)\dot{p}^{Sc}\right] = 0 \tag{48}$$

where $c^s = \frac{\partial S^l}{\partial p^c}$ is the specific moisture capacity and $p^c = p^{Sc} - p^l$ is the capillary pressure.

5.3.2. Fluid phase

Using Equation (37), the balance equation for fluid component can be described as:

$$\frac{\partial \boldsymbol{\phi}^l \rho_l^l}{\partial t} + \boldsymbol{\phi}^l \rho_l^l \ \ \cdot \mathbf{v}^s + \ \ \cdot \mathbf{I}^l = 0. \tag{49}$$

Then, by using Eqs. and the relationship between the chemical potential, temperature, molar mass, and universal gas constant (Katchalsky and Peter 1965, Chen *et al.* 2018) the final governing equation for the liquid phase is as follows:

$$\zeta S^l \ \ \cdot \dot{\mathbf{d}} + \left(\frac{\zeta - \phi}{K^s} S^l S^l + S^l \frac{\phi}{K^w}\right)\dot{p}^l + \frac{\zeta - \phi}{K^s} S^l S^{Sc} \dot{p}^{Sc} + \left(-\frac{\zeta - \phi}{K^s} S^l p^c + \phi\right)\dot{S}^l + \left[- \ \cdot k_{abs}\frac{k_{rl}}{v^l}\left(\ p^l - r_1 \frac{\rho_l^l}{\rho_{Sc}^{Sc}} \ p^{Sc} - r_2 \rho_l^l \frac{1}{c^w c^c}\frac{RT}{M^c} \ c^c\right)\right] = 0 \tag{50}$$

where M^c is the molar mass, R is the universal gas constant, and K^w and K^s are the bulk modulus of water and the solid, respectively.

Similarly, the governing equation for the supercritical phase can be written as

$$\zeta S^{Sc} \ \ \cdot \dot{\mathbf{d}} + \left(\frac{\zeta - \phi}{K^s} S^{Sc} S^{Sc} + S^g \frac{\phi}{K^{Sc}}\right)\dot{p}^{Sc} + \frac{\zeta - \phi}{K^s} S^{Sc} S^l \dot{p}^l + \left(\frac{\zeta - \phi}{K^s} S^{Sc} p^c + \phi\right)\dot{S}^{Sc} + \left[- \ \cdot k_{abs}\frac{k_{rSc}}{v^{Sc}}\left(\ p^{Sc} - r_3 \frac{\rho_{Sc}^{Sc}}{\rho_l^l} \ p^l - r_4 \rho_{Sc}^{Sc} \frac{1}{c^w c^c}\frac{RT}{M^c} \ c^c\right)\right] = 0 \tag{51}$$

where K^{Sc} is the bulk modulus of $ScCO_2$.

5.3.3. Chemical phase

The governing equation for the chemical transport (dissolved salt) can be derived using Eq. (11):

$$\dot{\rho}^c + \rho^c \quad \cdot \mathbf{v}^c + \quad \cdot \mathbf{I}^c = 0. \tag{52}$$

By using Equation. (2), (7), (13), and (24) and assuming a small deformation ($J = 1$), the final governing equation for the chemical transport (salt) can be written as:

$$\left(\phi S^l \rho_l^l\right)\dot{c}^c + \rho_l^l \mathbf{u}^l \cdot \quad c^c + \quad \cdot \mathbf{J}^c = 0. \tag{53}$$

5.3.4. Extra terms and novelty

The final derived governing equations for the liquid and supercritical phases are relatively similar to the classic transport equations for two-phase transport introduced by other researchers (Schrefler and Xiaoyong 1993, Islam *et al.* 2020, Abdullah *et al.* 2022). Nevertheless, there are new coupling terms introduced in Equations (50) and (51) that did not exist in the previous research. For example, in the literature, the Darcy flow term only contains the pressure of the liquid (e.g. $\cdot k_{abs}\frac{k_{rl}}{\nu^l}\left(\quad p^l\right)$), but in Equation (50), new terms are added. The first is the coupling term $-r_3\frac{\rho_{Sc}^{Sc}}{\rho_l^l} \quad p^l$, that determines the dissipation energy from the liquid flow due to the supercritical/liquid interaction (friction). The second term $-r_4\rho_{Sc}^{Sc}\frac{1}{c^w c^c}\frac{RT}{M^c} \quad c^c$ represents the coupling relation between the solute in the liquid, supercritical fluid density, and liquid (saline water) flow. This term was used in some papers to determine the osmosis effect on the transport in very low permeability conditions (Chen *et al.* 2018). Therefore, it is anticipated that the effect of this parameter on pressure, temperature, and mechanical deformation would be relatively lesser than the impact of the friction parameter.

The following section details the sensitivity effect of these terms on the main dependent variables, such as pressure and displacement of solid porous media, and the estimates of r_1 and r_3. Parameters r_2 and r_4 are expected to have a negligible effect due to the low energy dissipated during chemical transport. Moreover, the terms of the chemical dissipation energy could be useful when caprock leakage is investigated (low permeability) or when osmosis is present.

Finally, in the proposed model, the coupling term between the transport equations of two-phase is derived using the thermodynamics framework. This approach ensures that the equations are more rigorous and systematic, as the entire constitutive model can be obtained using a single driving force 'entropy production'. In contrast, other research in the field, such as the work by Qiao *et al.* (2018), has used additional coefficients to represent the mechanical influence between phases in their equations.

6. Validation and numerical simulation

This part of the article is divided into two sections: (6.1) validation of the general equations and (6.2) sensitivity analysis for the new friction term parameters r_1 and r_3.

6.1. General model validation

The model is validated against results from experimental works reported in the literature, and the effect and importance of the new extra terms are discussed in the sensitivity analysis section. First, the constitutive equations are solved numerically using the finite element method. Unfortunately, limited documented experiments have been conducted for a two-phase flow in a deforming porous medium. Since there is no analytical solution for such a complicated system, some researchers have attempted to validate their mathematical models by comparing them to results of known cases (Meiri 1981, Schrefler and Xiaoyong 1993, Gawin and Sanavia 2009).

Liakopoulos (1965b) conducted an experiment consisting of a column filled with a porous material to investigate water transport under unsaturated conditions. This experiment became a benchmark, with many researchers, such as (Narasimhan and Witherspoon 1978, Gawin *et al.* 1997, Schrefler and Scotta 2001, Laloui *et al.* 2003, Hu *et al.* 2011, Kim and Kim 2013, Islam *et al.* 2020, Wei *et al.* 2020, Abdullah *et al.* 2022), using the drainage experiment to validate their mathematical models.

In this study, the drainage experiment (Liakopoulos 1965b) is used to test the general governing equations of the fully coupled framework model and confirm that the new terms do not cause numerical issues. The model is solved numerically using COMSOL Multiphysics® (COMSOL, Inc.) software, and the results are compared to experimental data. COMSOL Multiphysics is a numerical software that is widely used in both the academic and industrial filed to solve relatively complex models using the finite element method. COMSOL Multiphysics was chosen due to its flexibility in customising equations, its inherent Multiphysics capabilities, and the trustworthiness it demonstrated in previous benchmark studies. This adaptability was essential given the uniqueness of the research parameters and the need for specific modifications. In this model, both the Darcy law physics and solid mechanics physics were adjusted, and equations were solved using an extra-fine triangle mesh setting. Liakopoulos only measured the liquid-phase pressure (water) and did not include data for the gas phase (air pressure), the Schrefler and Scotta (2001) numerical results are used. Moreover, no chemical was included in this experiment. Nevertheless,

because this simulation aims to test the effect of the new governing equations terms, the simulation results can be compared to the experiment and other results.

6.2. Drainage test experiment

The Liakopoulos experiment consisted of a sand column (Perspex and Del Monte sand). The tube column was 1.0 m long and 10 cm in diameter. The bottom of the column was exposed to atmospheric pressure, and the tube wall was assumed to be rigid and impermeable.

Tensiometers were used to measure the pore pressure change with column height. The column was fed with water from the top to ensure a constant flow rate throughout the column. When the drainage water at the bottom became equal to the filling rate, the water flow supply from the top was stopped and the experiment started (considered as $t = 0$). The water continued draining from the tube due to gravity.

Water pressure measurements were taken at various times ($t = 5$, 10, 20, 30, 60, and 120 min). The water saturation and relative permeability were calculated based on capillarity pressure according to the Brooks and Corey (1966) model as follows:

$$S^w = 1 - 0.10152\left(\frac{p^c}{\rho_t^w g}\right)^{2.4279}, k_{\mathrm{rw}} = 1 - 2.207(1 - S^w)^{1.0121}. \tag{54}$$

The above equations are valid in a porous medium with water saturation $S^w > 0.91$ and capillary pressure $p^c > 0$. Moreover, for the numerical simulation, some assumptions were set to ensure a stable numerical solution:

(i) The drainage flow occurs due to gravity and is in the vertical direction only.
(ii) When the experiment starts ($t = 0$), the sand column is fully saturated ($S^w = 1$).
(iii) The porosity value does not change during the experiment.

Table 1 summarises the material data used for the numerical simulation. For parameters not provided by Liakopoulos, such as Young's modulus and Poisson's ratio, values estimated by other researchers were used (Schrefler and Xiaoyong 1993, Schrefler and Scotta 2001). Figure 1 shows the initial and boundary conditions used in the numerical simulation.

Equations (50) and (51) contain the four parameters r_1, r_2, r_3, and r_4. These parameters must be obtained by laboratory testing; for now, the values will be estimated by trial and error. Parameters r_1 and r_3 relate to the first new term that represents the effect of the entropy generated by the two-phase interaction, whereas r_2 and r_4 are linked to the loss caused by chemical transport in the system. It has been observed, as discussed in the following section, that parameters r_1 and r_3 have a more significant impact on pressure behaviour than r_2 and r_4. This is because the entropy generated due to the transport of such a small amount of chemical (NaCl has a mass fraction of 0.1) is almost negligible; however, the friction induced by the interaction between the multi-phase flows is much higher. Parameters r_1 and r_3 need to be estimated based on the fluids, porous medium, and experimental setup. Figure 2 shows the numerical results of the water pressure of the proposed coupled model compared to the experimental results. The simulation was in good agreement with the experimental measurements. However, at the start of the experiment ($t = 5$ and 10 min), there was a shift in the water pressure, which other researchers experienced when comparing their models to the experiment (Schrefler and Xiaoyong 1993, Schrefler and Scotta 2001, Islam *et al.* 2020).

Figure 3, Figures 5 , and 6 show the numerical results of the proposed model compared with the Schrefler and Scotta (2001) model. Figure 4 shows a 2D plot of the air pressure moving through the column at various times. In Figure 3, the peak pressure moves more aggressively across the sand column, with higher pressure values.

Table 1. Parameters used for the Liakopoulos drainage test (Liakopoulos 1965b.).

Physical meaning	Reference	Values and units
Young's modulus	(Schrefler and Scotta 2001)	$E = 1.3$ MPa
Water density	(Schrefler and Scotta 2001)	$\rho_w^w = 1000$ kg/m^3
Gas density (air)	(Schrefler and Scotta 2001)	$\rho_g^g = 1.2$ kg/m^3
Solid density (sand)	(Schrefler and Scotta 2001)	$\rho^s = 2000$ kg/m^3
Poisson's ratio	(Schrefler and Scotta 2001)	$\theta = 0.4$
Biot's coefficient	(Schrefler and Scotta 2001)	$\zeta = 1$
Porosity	(Schrefler and Scotta 2001)	$\phi = 0.2975$
Intrinsic permeability of the solid (sand)	(Schrefler and Scotta 2001)	$k_{abs} = 4.5 \times 10^{-13}$ m^2
Dynamic viscosity of water	(Schrefler and Scotta 2001)	$v^w = 1 \times 10^{-3}$ Pa.s
Dynamic viscosity of gas (air)	(Schrefler and Scotta 2001)	$v^g = 1.8 \times 10^{-5}$ Pa.s
Bulk modulus of water	(Schrefler and Scotta 2001)	$K_w = 2.0 \times 10^3$ MPa
Bulk modulus of gas (air)	(Schrefler and Scotta 2001)	$K_g = 0.1$ MPa
Bulk modulus of solid (sand)	(Schrefler and Scotta 2001)	$K_s = 1.0 \times 10^6$ MPa

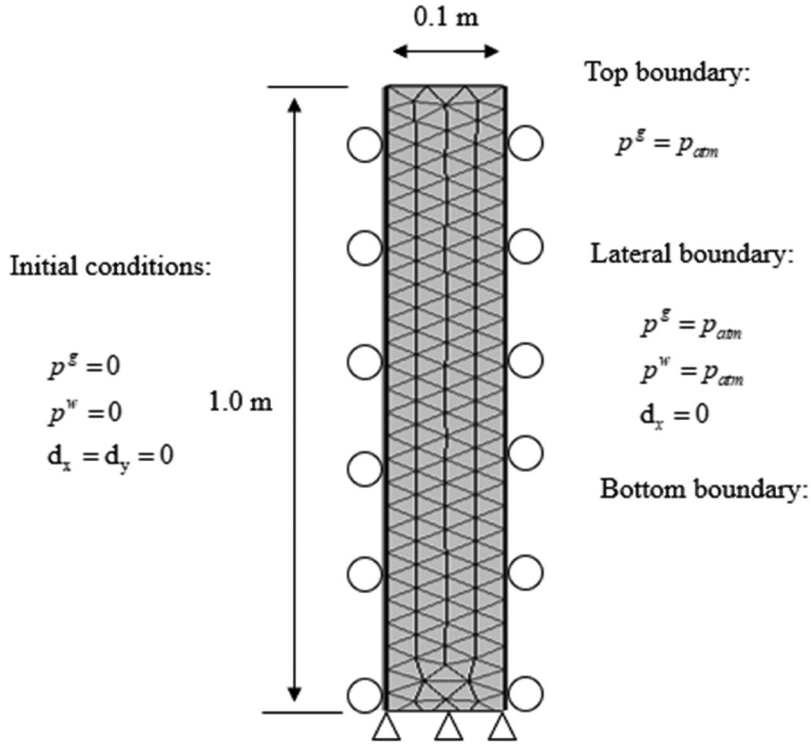

Figure 1. Initial and boundary conditions for Liakopoulos drainage test (Liakopoulos 1965b).

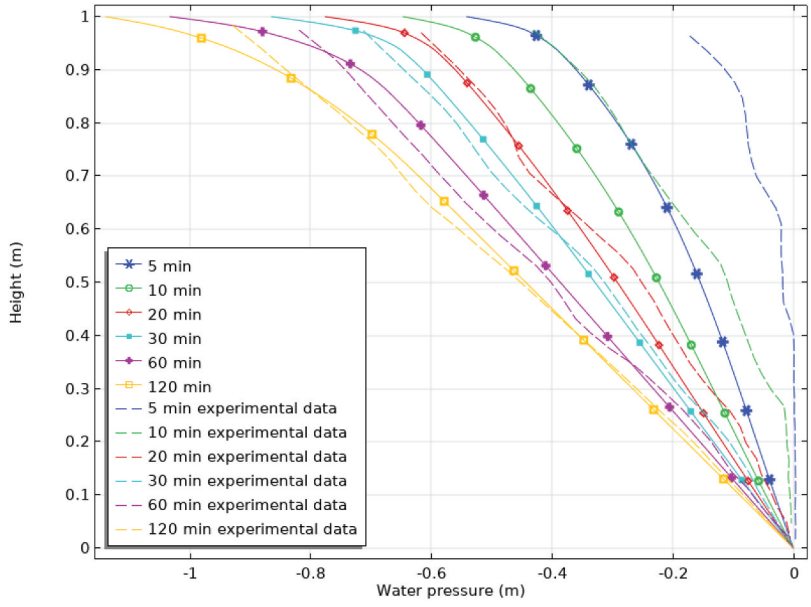

Figure 2. Liakopoulos (1965b) experiment vs simulation results of liquid pressure (p^l) distributed through sand column at different times.

This behaviour was observed and discussed by Schrefler and Scotta (2001), who compared it with other researchers. Hu *et al.* (2011) obtained results that are more similar to our simulation results, which is due to the assumptions made regarding boundary conditions. In this simulation, the space between the sand and the tube walls was assumed to be gas permeable, while in the original experiment, the boundary condition was based on the gas-tight assumption. However, researchers such as Hu *et al.* (2011) obtained a better match with the experiment when the gas was assumed to have fair passage between the sand and inner wall of the tube. This could be an experimental error in which the space between the inner wall and filling sand was not 100%

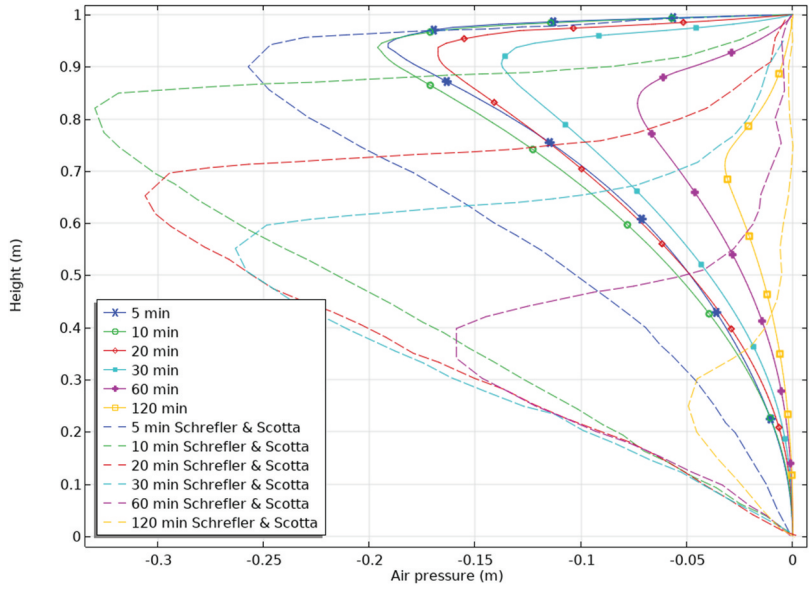

Figure 3. Simulation and Schrefler and Scotta (2001) results for air pressure (p^g).

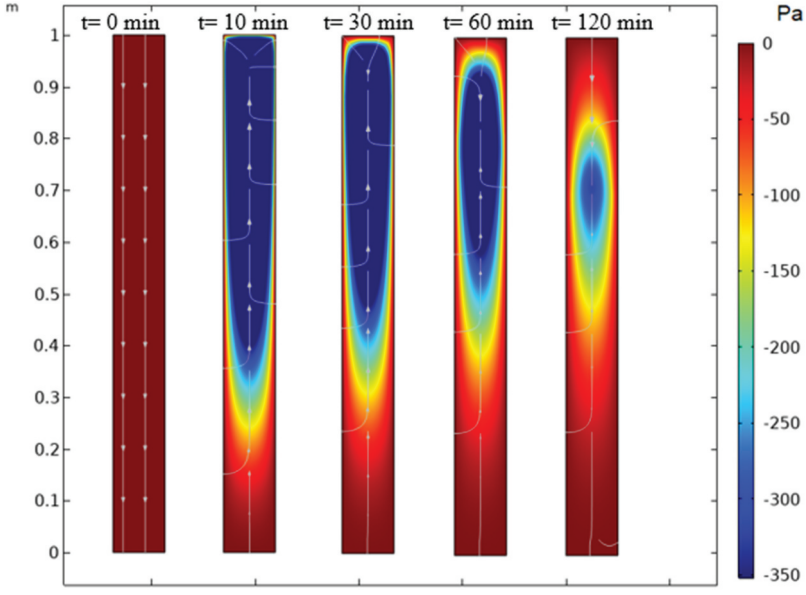

Figure 4. Air pressure (p^g) distribution at 0, 10, 30, 60, and 120 min.

insulated. Figure 4 shows a 2D graph of the air leaking from the sides into the porous medium.

Figure 5 shows the water saturation of the sand column. Unfortunately, Liakopoulos (1965a) did not measure the saturation in his experiment, and thus it is not possible to compare the values to the experiment's results. The difference between the simulation results and Schrefler and Scotta (2001) is partially due to the difference in the gas pressure values. That is because the water saturation is a function of the capillary pressure, which is the difference between the gas pressure and the water pressure.

Figure 6 displays the mechanical deformation of the sand. The simulation results exhibit qualitative similarity to (Schrefler and Scotta 2001), although the magnitude is shifted by approximately 0.1 mm (36% less). This difference may be attributed to the variation in the boundary condition, which affected the gas pressure

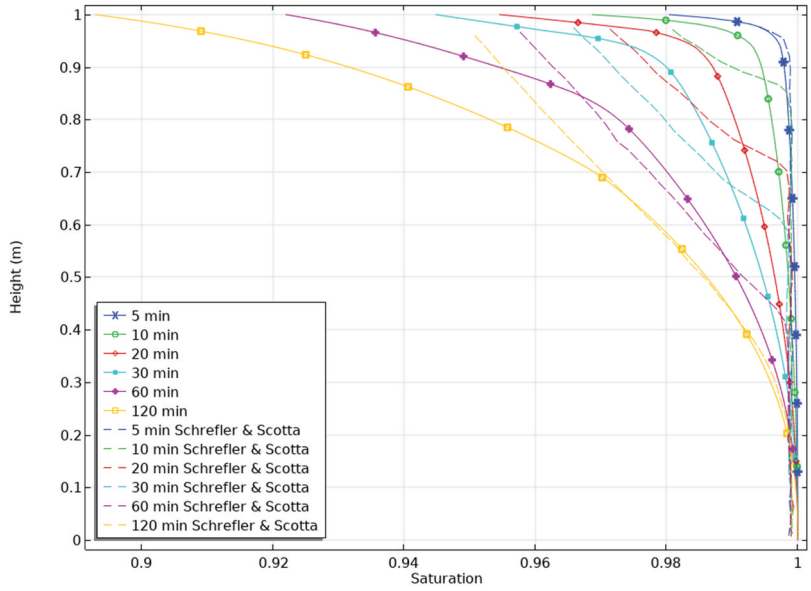

Figure 5. Simulation and Schrefler and Scotta (2001) results for liquid saturation (S^l).

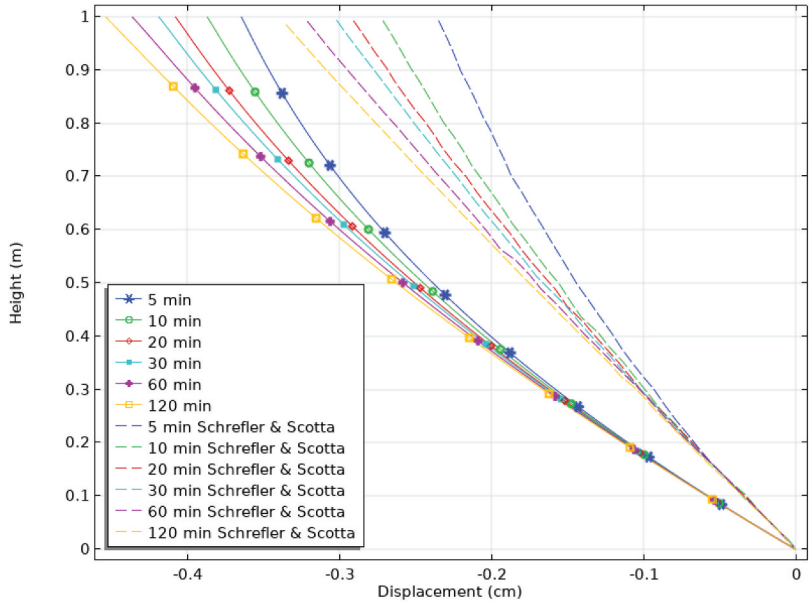

Figure 6. Simulation and Schrefler and Scotta (2001) results for mechanical deformation of porous medium.

and hence the mechanical deformation. It is worth noting that other researchers (Islam *et al.* 2020) have reported results closer to our simulation.

Figure 7 and Figure 8 show the chemical transport (NaCl) in the system at different times. As expected, the mass fraction of the sodium chloride was transported from the top to the bottom of the column. The effect of transporting such a low concentration of chemical in a low water flow (only gravity was considered) is minor. However, for the case of carbon dioxide injection under high pressure and a higher chemical concentration (salts and minerals), the coupling effect of the chemical transport is expected to be higher.

6.3. Sensitivity analysis

In this section, a sensitivity analysis for the new parameters r_1 and r_3 is conducted to assess their impact on the

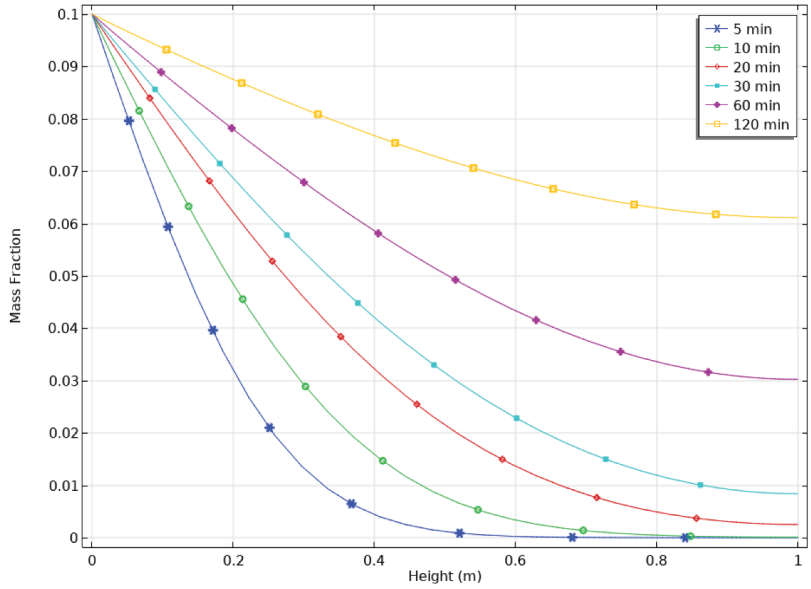

Figure 7. Mass fraction change due to diffusion (chemical transport) in sand column.

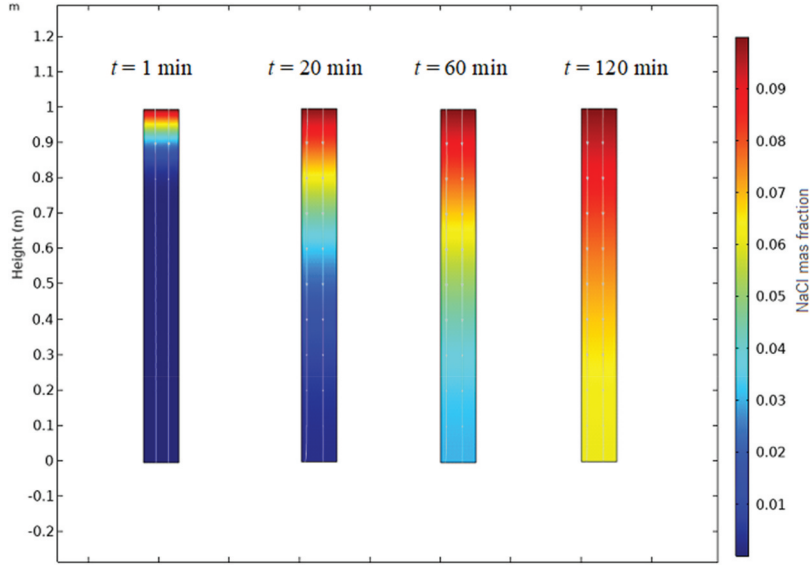

Figure 8. Chemical concentration (mass fraction of NaCl) distribution at 1, 20, 60, and 120 min.

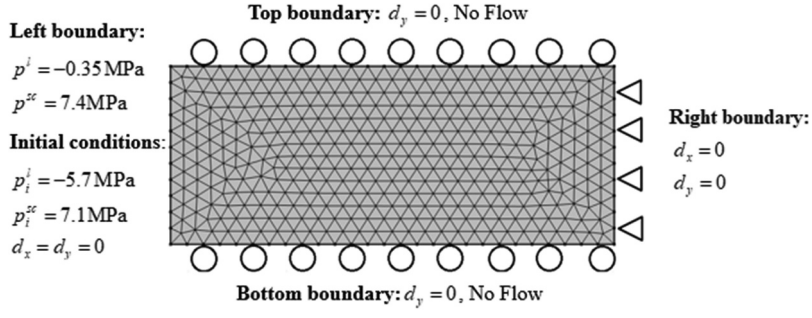

Figure 9. Initial and boundary conditions of rock sample.

transport process. To simplify the discussion, a conceptional 2D model is considered. The model is 50 cm × 20 cm of porous media (limestone rock sample). The initial and boundary conditions are shown in Figure 9. For water saturation calculations, the Van Genuchten relationship is used as:

$$k_{rw} = (S^w)^{0.5} \times \left[1 - \left(1 - \left((S^w)^1\right)\right)^m\right]^2 \quad (55)$$

where the water saturation can be calculated by:

$$S^w = \left[\left(-\frac{p^c}{M}\right)^{\frac{1}{1-m}} + 1\right]^{-m} \quad (56)$$

M and m are Van Genuchten parameter. The parameters of the model were obtained from the literature and are listed in Table 2.

In this analysis, parameters r_1 and r_3 were simulated at different values to discern their impact on the results. When a value was given to one parameter, the other is assumed to be zero. The selection of these values is primarily driven by a trial-and-error process. By exploring a range of values, we identify the maximum and minimum thresholds at which the model converged. This approach is taken due to the absence of available experimental data for these phenomenological coefficients, and hence, trial-and-error provides a means to approximate these limits which are found to be $r_1, r_3 = 0.01\tilde{0}.1$.

Considering the compact size of the rock sample and the heightened pressure of the fluid, we assume the permeability to be minimal. Such an assumption guarantees that the fluid flows at a satisfactory rate, preventing it from rapidly reaching equilibrium. Figures 10–12 show the liquid pressure, supercritical pressure, and solid deformation for r_1 and r_3 values of 0.01 and 0.1, respectively. The data displayed corresponds to the

Table 2. Rock sample parameters.

Physical meaning	Reference	Values and units
Young's modulus	(Zhou and Burbey 2014)	$E = 33$ GPa
Water density	(Zhou and Burbey 2014)	$\rho_w^w = 1000\,\mathrm{kg/m^3}$
$ScCO_2$ density	(Zhou and Burbey 2014)	$\rho_{Sc}^{Sc} = 660\,\mathrm{kg/m^3}$
Solid density	(Zhou and Burbey 2014)	$\rho^s = 2600\,\mathrm{kg/m^3}$
Poisson's ratio	(Zhou and Burbey 2014)	$\theta = 0.26$
Biot's coefficient	(Chen *et al.* 2016)	$\zeta = 1$
Porosity	(Zhou and Burbey 2014)	$\phi = 0.123$
Intrinsic permeability of the solid	(Assumed)	$k_{abs} = 1.4 \times 10^{-20}$ m^2
Dynamic viscosity of water	(Zhou and Burbey 2014)	$v^w = 1 \times 10^{-3}$ Pa s
Dynamic viscosity of $ScCO_2$	(Zhou and Burbey 2014)	$v^{Sc} = 6 \times 10^{-5}$ Pa s
Bulk modulus of water	(Zhou and Burbey 2014)	$K_w = 2.2 \times 10^3$ MPa
Bulk modulus of $ScCO_2$	(Zhou and Burbey 2014)	$K_{Sc} = 58$ MPa
Bulk modulus of solid	(Zhou and Burbey 2014)	$K_s = 74$ GPa
Van Genuchten parameter	(Chen *et al.* 2016)	$m = 0.43$
Van Genuchten parameter	(Chen *et al.* 2016)	$M = 51$ MPa

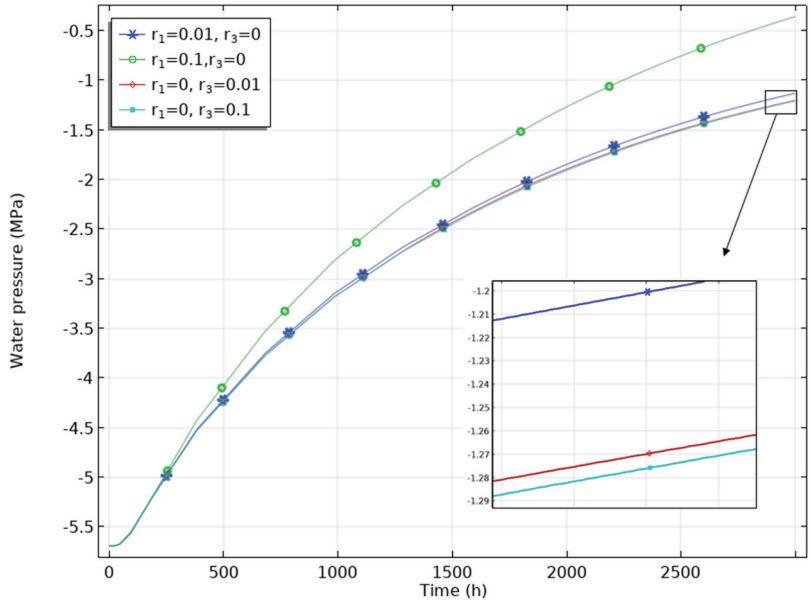

Figure 10. Water pressure at coordinate point (0.1,0.25) at different r_1 and r_2 values.

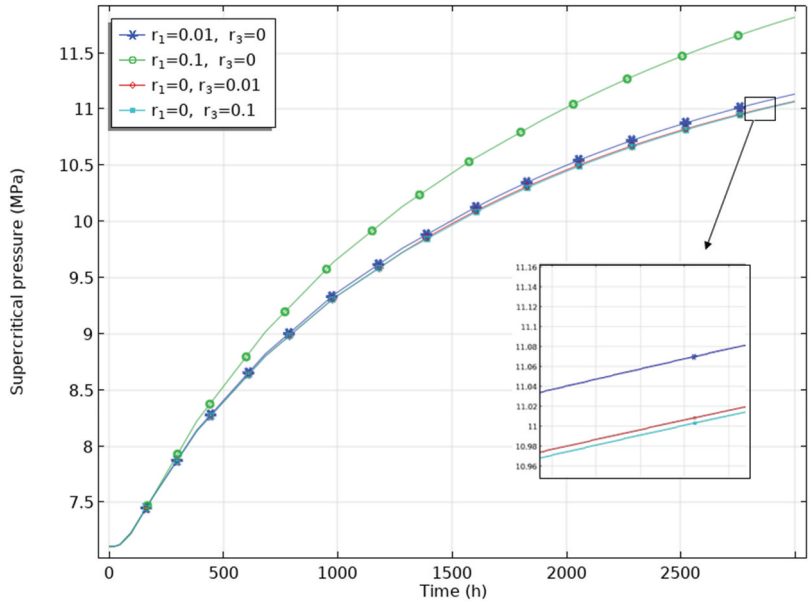

Figure 11. Supercritical pressure at coordinate point (0.1,0.25) at different r_1 and r_2 values.

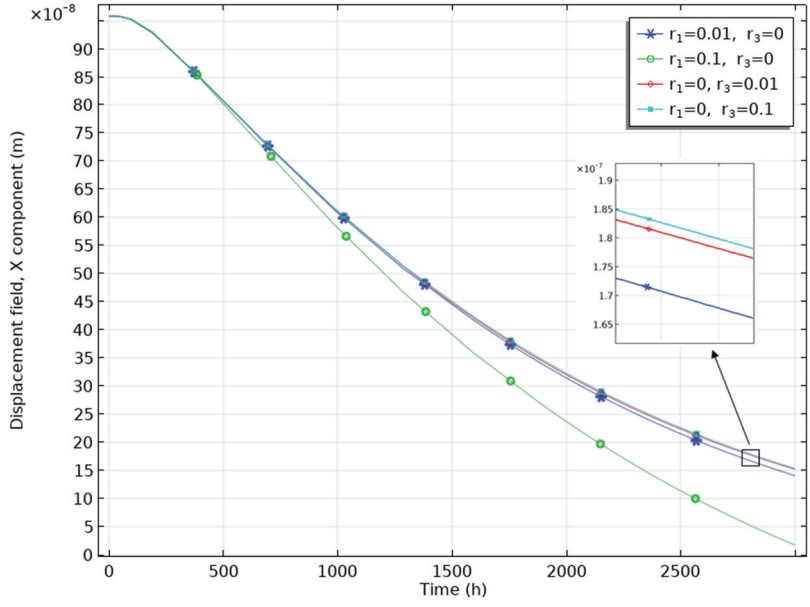

Figure 12. Horizontal deformation at coordinate point (0.1,0.25) at different r_1 and r_2 values.

coordinate point (0.1, 0.25), centrally located within the conceptual 2D model. Parameter r_1 in the governing equation for the liquid relates directly to the supercritical flow's impact on the liquid flow. Notably, the figures reveal that the influence of r_1 is greater than r_3. This prominence arises from the elevated water saturation value, resulting in a reduced saturation level for the supercritical phase ($S^l + S^{Sc} = 1$). Since the saturation value aligns with the capillary pressure (as detailed in the Van Genuchten relations), it is contingent on both initial and boundary conditions.

In Figure 13, which shows water saturation exceeding 96%, we delve deeper into the implications of this saturation: the energy losses stemming from the interaction between the two-phase flow correlate directly with the fluid volume present within the pore (saturation). The role of r_1 lead to increment in liquid and supercritical pressure. Upon closer inspection, an

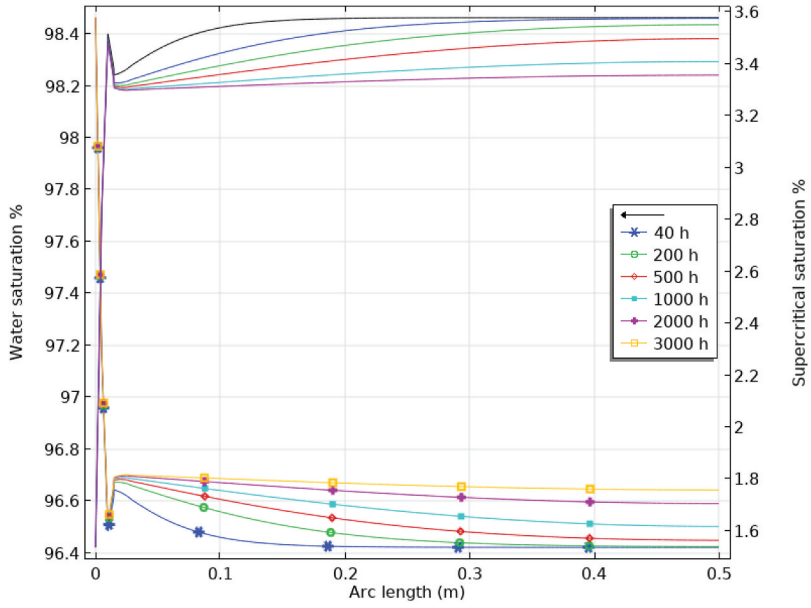

Figure 13. Supercritical and water saturation across horizontal section of sample at $r_1 = r_2 = 0$.

elevation in r_1 values lead to an increase in both the liquid and supercritical pressures, suggesting diminished energy losses from fluid interactions.

Figure 14–16 probe deeper into the sensitivities of parameters r_1 and r_3 across a horizontal cross-section of the sample at the 2000-h mark. From a detailed examination, one discernible pattern is the apex of these parameters' influence post-entry into the formation, a crucial juncture where the two flows converge and begin mixing. This observation implies a localised, maximum interaction effect right after entry, which then diminishes as the fluids travel deeper, hinting at lessening interactions or stabilisation of the two fluids over distance.

The modulation of these parameters indeed has pronounced effects on the outcomes. However, these impacts are intrinsically tied to the saturation value. For instance, r_3's sway is more pronounced when water saturation nears the supercritical saturation, a fact buttressed by Equation (50). Here, the relative permeabilities for water and the supercritical phase get multiplied by r_1 and r_3, respectively. On the

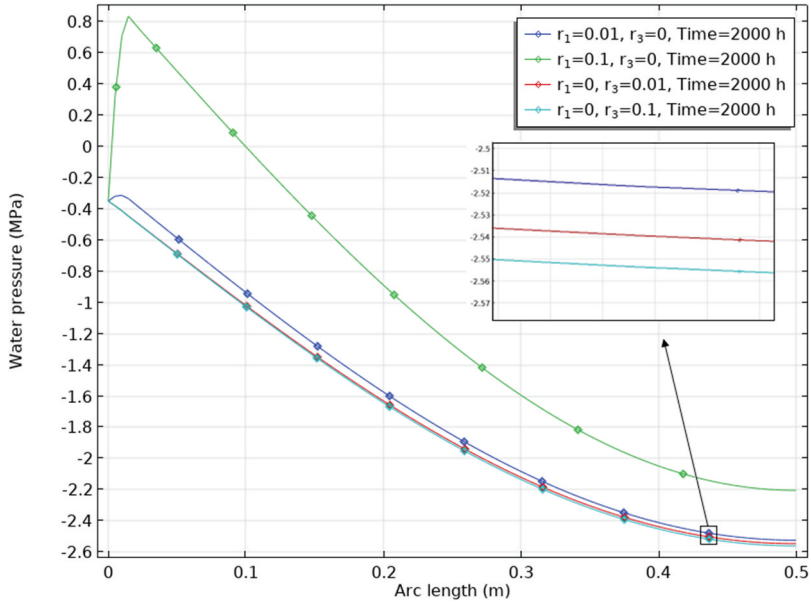

Figure 14. Water pressure across horizontal section of sample at different r_1 and r_2 values.

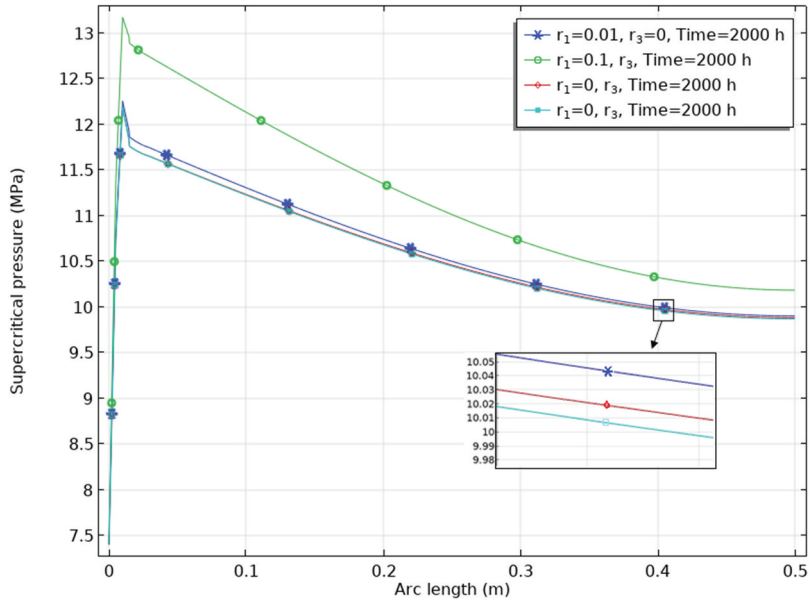

Figure 15. Supercritical pressure across horizontal section of sample at different r_1 and r_2 values.

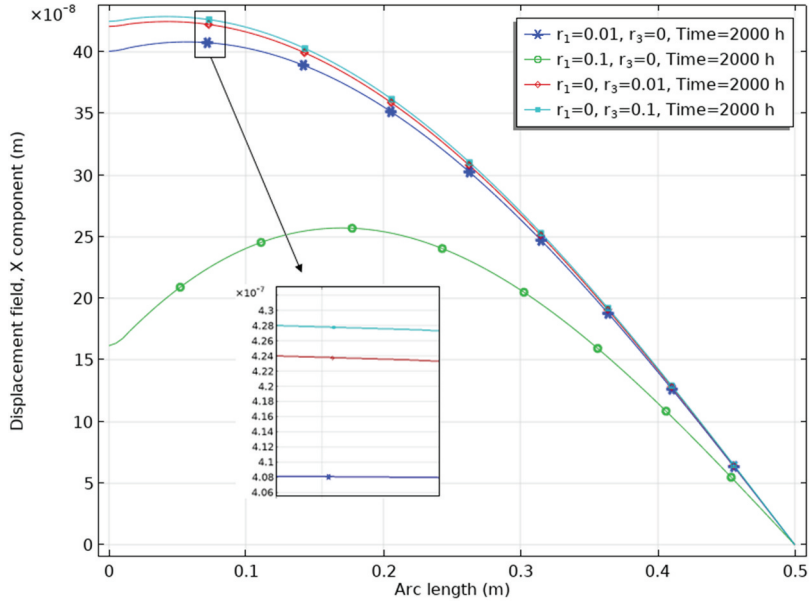

Figure 16. Deformation across horizontal section of sample at different r_1 and r_2 values.

other hand, parameter r_3, present in the supercritical phase's governing equation and associated with the liquid's effect on the supercritical phase, registers negligible influence on the results.

Finally, delving into the second term of the governing equation, we underscore the minuscule role of chemical entropy. It gains relevance predominantly in scenarios marked by low permeability or evident osmosis. Yet, this term stands as a potential indicator for tracking carbon dioxide leakage via low-permeability caprock resulting from osmosis.

7. Conclusion

A fully coupled multi-phase HM-supercritical-chemical constitutive framework under isothermal conditions is developed based on the mixture coupling theory. The

phenomenological equations are used to establish two new terms describing the coupled interaction between supercritical and liquid phases and chemical solute transport. The model also considers the coupling between the deformation of a solid and the change in pressure. The coupled model is based on Helmholtz's free energy equations and Biot's poroelasticity model. Experimental data were used to validate the model. COMSOL Multiphysics® software was used to numerically solve the model through the finite element method. The numerical simulation results are in good agreement with the experimental results. The sensitivity analysis shows that the effect of the new terms is highly dependent on the relative permeability, which can be directly related to the saturation value. A sensitivity analysis also shows that the value of the new terms parameters r_1 and r_3 has a significant impact on the pressures and deformation if the saturation of the phase is high. The solute transport parameters r_2 and r_4 seem to have less influence. However, these terms are useful when investigating the osmosis effect or when carbon dioxide leakage through a low permeability caprock is considered. In this model, only one solute was simulated; however, for a larger field, such as carbon sequestration in a large formation, with more solutes present, a more significant impact is predicted.

The significance of this paper is its inclusion of energy dissipation due to both friction and solute transport in two-phase interactions, influencing pressure, flow rate, and fluid distribution. More experiments are needed to refine 'r' parameters at diverse injection rates. The results are markedly influenced by dynamic viscosity, a vital element in the abnormal behaviour of supercritical carbon dioxide.

List of notations

$\mathbf{d}$	Displacement tensor
c^s	Specific moisture capacity
c^w	Chemical concentration of water
c^c	Chemical concentration of the solute
$\mathbf{E}$	Green strain
E	Young modulus
$\mathbf{F}$	Deformation gradient
G	The rock's shear modulus
$\mathbf{I}$	Unit tensor
$\mathbf{I}^\beta$	Mass flux of the phase/species
J	Jacobian
$\mathbf{J}^\beta$	Diffusion flux
K	Rock's Bulk modulus
k_{abs}	Intrinsic permeability
K^s	Bulk modulus of the solid matrix
K^β	Bulk modulus of the phase/species
$k_{r\beta}$	Phase/species relative permeability
m^β	mass density of the phase flows in the reference configuration
M^c	Molar mass of the chemical solute
$\mathbf{n}$	The outward unit normal vector
R	universal gas constant
p^c	Capillary pressure
p^β	Phase/species pressure
p^p	Average pore pressure
S^β	Saturation of the phase/species
T	Constant temperature
$\mathbf{T}$	Second Piola-Kirchhoff stress tensor
t	Time
$\mathbf{u}^\beta$	Darcy velocity of the phase/species
V	Arbitrary microscopic domain
V^β	Volume occupied by phase/species
V^{pore}	Volume of the pore space
W	Dual potential
$\mathbf{v}^\beta$	Phase/species velocity
Γ	Boundary attached on the surface
β	Phase or species (s, w, l, Sc, c)
v^β	Phase/species viscosity
ρ_β^β	Phase density
ρ^β	Mixture density
ϕ^β	Phase volume fraction (phase porosity)
ϕ	Porosity
ψ	Helmholtz free energy density
ψ^{pore}	Helmholtz free energy density of the pore Constituent
Ψ	Free energy in the reference configuration
σ	Cauchy stress tensor
μ^β	Chemical potential of the phase
ε_{ij}	Strain tensor
σ	Cauchy stress tensor
γ	Entropy production per unit volume
υ	Porosity in the reference configuration
ζ	Biot's coefficient
θ	Poisson's ratio
	Gradient

Acknowledgments

The authors would like to thank the Kuwait Oil Company for its support and sponsoring this work; YM would like to thank the CERES studentship support from the school of civil engineering at the University of Leeds.

Disclosure statement

No potential conflict of interest was reported by the author(s).

Funding

This work was supported by the Kuwait Oil Company.

ORCID

Xiaohui Chen http://orcid.org/0000-0002-2053-2448

References

Abdullah, S., *et al*., 2022. A fully coupled hydro-mechanical-gas model based on mixture coupling theory. *Transport in Porous Media*, 143 (1), 1–22. doi:10.1007/s11242-022-01784-6

Alonso, J., *et al*., 2012. Hydro-mechanical analysis of CO_2 storage in porous rocks using a critical state model. *International Journal of Rock Mechanics and Mining Sciences*, 54, 19–26. doi:10.1016/j.ijrmms.2012.05.016

André, L., *et al*., 2007. Numerical modeling of fluid–rock chemical interactions at the supercritical CO_2 –liquid interface during CO_2 injection into a carbonate reservoir, the Dogger aquifer (Paris Basin, France). *Energy Conversion and Management*, 48 (6), 1782–1797. doi:10.1016/j.enconman.2007.01.006

Bao, J., Xu, Z., and Fang, Y., 2014. A coupled thermal-hydro-mechanical simulation for carbon dioxide sequestration. *Environmental Geotechnics*, 3 (5), 312–324. doi:10.1680/envgeo.14.00002

Brooks, R.H. and Corey, A.T., 1966. Properties of porous media affecting fluid flow. *Journal of the Irrigation and Drainage Division*, 92 (2), 61–88. doi:10.1061/JRCEA4.0000425

Chen, X., 2010. *Unsaturated hydro-chemo-mechanical modelling based on modified mixture theory*. Thesis (PhD). The University of Manchester (United Kingdom).

Chen, X., 2013. Constitutive unsaturated hydro-mechanical model based on modified mixture theory with consideration of hydration swelling. *International Journal of Solids and Structures*, 50 (20–21), 3266–3273. doi:10.1016/j.ijsolstr.2013.05.025

Chen, X. and Hicks, M.A., 2011. A constitutive model based on modified mixture theory for unsaturated rocks. *Computers and Geotechnics*, 38 (8), 925–933. doi:10.1016/j.compgeo.2011.04.008

Chen, X., *et al*., 2016. Unsaturated hydro-mechanical–chemical constitutive coupled model based on mixture coupling theory: hydration swelling and chemical osmosis. *International Journal of Engineering Science*, 104, 97–109. doi:10.1016/j.ijengsci.2016.04.010

Chen, X., Thornton, S.F., and Pao, W., 2018. Mathematical model of coupled dual chemical osmosis based on mixture-coupling theory. *International Journal of Engineering Science*, 129, 145–155. doi:10.1016/j.ijengsci.2018.04.010

Coussy, O., Dormieux, L., and Detournay, E., 1998. From mixture theory to Biot's approach for porous media. *International Journal of Solids and Structures*, 35 (34–35), 4619–4635. doi:10.1016/S0020-7683(98)00087-0

Fan, C., *et al*., 2019. Thermo-hydro-mechanical-chemical couplings controlling CH4 production and CO2 sequestration in enhanced coalbed methane recovery. *Energy*, 173, 1054–1077. doi:10.1016/j.energy.2019.02.126

Fan, C., *et al*., 2023. Recent Advances and perspectives of CO2-enhanced coalbed methane: experimental, modeling, and technological development. *Energy & Fuels*, 37 (5), 3371–3412. doi:10.1021/acs.energyfuels.2c03823

Gawin, D. and Sanavia, L., 2009. A unified approach to numerical modeling of fully and partially saturated porous materials by considering air dissolved in water. *Computer Modeling in Engineering & Sciences*, 53, 255.

Gawin, D., Simoni, L., and Schrefler, B., 1997. Numerical model for hydro-mechanical behaviour in deformable porous media: a benchmark problem. *Proceedings of the 9th International Conference on computer methods and advances in Geomechanics*, Wuhan, China, 1143–8.

Heidug, W. and Wong, S.W., 1996. Hydration swelling of water-absorbing rocks: a constitutive model. *International Journal for Numerical and Analytical Methods in Geomechanics*, 20 (6), 403–430. doi:10.1002/(SICI)1096-9853(199606)20:6<403:AID-NAG832>3.0.CO;2-7

Hu, R., Chen, Y., and Zhou, C., 2011. Modeling of coupled deformation, water flow and gas transport in soil slopes subjected to rain infiltration. *Science China Technological Sciences*, 54 (10), 2561–2575. doi:10.1007/s11431-011-4504-z

Islam, M., Huerta, N., and Dilmore, R., 2020. Effect of computational schemes on coupled flow and geomechanical modeling of CO_2 leakage through a compromised well. *Computation*, 8 (4), 98. doi:10.3390/computation8040098

Karrech, A., 2013. Non-equilibrium thermodynamics for fully coupled thermal hydraulic mechanical chemical processes. *Journal of the Mechanics and Physics of Solids*, 61 (3), 819–837. doi:10.1016/j.jmps.2012.10.015

Katachalsky, A. and Curran, P.F., 1965. *Nonequilibrium thermodynamics in biophysics*. Cambridge, MA: Harvard University Press.

Katchalsky, A. and Peter, F.C., 1965. *Frontmatter*. Cambridge (MA): Harvard University Press.

Kim, Y.-S. and Kim, J., 2013. Coupled hydromechanical model of two-phase fluid flow in deformable porous media. *Mathematical Problems in Engineering*, 2013, 1–8. doi:10.1155/2013/589452

Kueper, B.H. and Frind, E.O., 1991. Two-phase flow in heterogeneous porous media: 1. Model development. *Water Resources Research*, 27 (6), 1049–1057. doi:10.1029/91WR00266

Laloui, L., Klubertanz, G., and Vulliet, L., 2003. Solid–liquid–air coupling in multiphase porous media. *International Journal for Numerical and Analytical Methods in Geomechanics*, 27 (3), 183–206. doi:10.1002/nag.269

Lewis, R.W. and Schrefler, B.A., 1987. The finite element method in the deformation and consolidation of porous media.

LI, C. and Laloui, L., 2016a. Coupled multiphase thermo-hydro-mechanical analysis of supercritical CO_2 injection: benchmark for the in Salah surface uplift problem. *International Journal of Greenhouse Gas Control*, 51, 394–408. doi:10.1016/j.ijggc.2016.05.025

Li, C. and Laloui, L., 2016b. Coupled multiphase thermo-hydro-mechanical analysis of supercritical CO 2 injection: benchmark for the in Salah surface uplift problem. *International Journal of Greenhouse Gas Control*, 51, 394–408. doi:10.1016/j.ijggc.2016.05.025

Liakopoulos, A. 1965a. *Transient flow through unsaturated porous media* [Ph. D. thesis]. University of California, Berkeley, Calif, USA.

Liakopoulos, A. 1965b. *Transient flow through unsaturated porous media, D. Eng.* dissertation, Univ. of Calif, Berkeley.

Liu, A., *et al.*, 2021. Water sorption on coal: effects of oxygen-containing function groups and pore structure. *The International Journal of Coal Science & Technology*, 8 (5), 983–1002. doi:10.1007/s40789-021-00424-6

Liu, F., *et al.*, 2011. Coupled reactive flow and transport modeling of CO_2 sequestration in the Mt. Simon sandstone formation, Midwest U.S.A. *International Journal of Greenhouse Gas Control*, 5 (2), 294–307. doi:10.1016/j.ijggc.2010.08.008

Liu, T., *et al.*, 2021. Mechanical criterion for coal and gas outburst: a perspective from multiphysics coupling. *The International Journal of Coal Science & Technology*, 8 (6), 1423–1435. doi:10.1007/s40789-021-00447-z

Lu, W. and Zhang, X., 2020. Coupled thermo-hydro-mechanical modelling of carbon dioxide sequestration in saline aquifers considering phase change. *Current Science*, 119 (6), 973. doi:10.18520/cs/v119/i6/973-983

Ma, Y., Chen, X.-H., and Yu, H.-S., 2020. An extension of Biot's theory with molecular influence based on mixture coupling theory: mathematical model. *International Journal of Solids and Structures*, 191-192, 76–86. doi:10.1016/j.ijsolstr.2019.11.015

Meiri, D., 1981. Two-phase flow simulation of air storage in an aquifer. *Water Resources Research*, 17 (5), 1360–1366. doi:10.1029/WR017i005p01360

Narasimhan, T.N. and Witherspoon, P., 1978. Numerical model for saturated-unsaturated flow in deformable porous media: 3. Applications. *Water Resources Research*, 14 (6), 1017–1034. doi:10.1029/WR014i006p01017

Nasvi, M., *et al.*, 2013. Sub-and super-critical carbon dioxide permeability of wellbore materials under geological sequestration conditions: an experimental study. *Energy*, 54, 231–239. doi:10.1016/j.energy.2013.01.049

Qiao, Y., *et al.*, 2018. A mixture theory approach to model co- and counter-current two-phase flow in porous media accounting for viscous coupling. *Advances in Water Resources*, 112, 170–188. doi:10.1016/j.advwatres.2017.12.016

Richards, L.A., 1931. Capillary conduction of liquids through porous mediums. *Physics*, 1 (5), 318–333. doi:10.1063/1.1745010

Sasaki, K., *et al.*, 2008. Numerical simulation of supercritical CO_2 injection into subsurface rock masses. *Energy Conversion and Management*, 49 (1), 54–61. doi:10.1016/j.enconman.2007.05.015

Schrefler, B.A. and Scotta, R., 2001. A fully coupled dynamic model for two-phase fluid flow in deformable porous media. *Computer Methods in Applied Mechanics and Engineering*, 190 (24–25), 3223–3246. doi:10.1016/S0045-7825(00)00390-X

Schrefler, B.A. and Xiaoyong, Z., 1993. A fully coupled model for water flow and airflow in deformable porous media. *Water Resources Research*, 29 (1), 155–167. doi:10.1029/92WR01737

Siddiqui, M.A., Regenauer-Lieb, K., and Roshan, H., 2023. Thermo-Hydro-Chemo-Mechanical (THCM) continuum modelling of subsurface rocks: a focus on thermodynamics-based constitutive models. *Applied Mechanics Reviews*, 76 (3), 1–62. doi:10.1115/1.4056726

Siqueira, T.A., Iglesias, R.S., and Ketzer, J.M., 2017. Carbon dioxide injection in carbonate reservoirs – a review of CO_2 -water-rock interaction studies. *Greenhouse Gases: Science and Technology*, 7 (5), 802–816. doi:10.1002/ghg.1693

Taron, J. and Elsworth, D., 2009. Thermal–hydrologic–mechanical–chemical processes in the evolution of engineered geothermal reservoirs. *International Journal of Rock Mechanics and Mining Sciences*, 46 (5), 855–864. doi:10.1016/j.ijrmms.2009.01.007

Voskov, D.V., Henley, H., and Lucia, A., 2017. Fully compositional multi-scale reservoir simulation of various CO_2 sequestration mechanisms. *Computers & Chemical Engineering*, 96, 183–195. doi:10.1016/j.compchemeng.2016.09.021

Wei, H., *et al.*, 2020. A naturally stabilized semi-Lagrangian meshfree formulation for multiphase porous media with application to landslide modeling. *Journal of Engineering Mechanics*, 146 (4), 04020012. doi:10.1061/(ASCE)EM.1943-7889.0001729

Wolf, J.L., *et al.*, 2016. Benefits and restrictions of 2D reactive transport simulations of CO_2 and SO_2 co-injection into a saline aquifer using TOUGHREACT V3. 0-OMP. *International Journal of Greenhouse Gas Control*, 54, 610–626. doi:10.1016/j.ijggc.2016.07.005

Wriggers, P., 2008. *Nonlinear finite element methods*. Berlin Heidelberg: Springer Science & Business Media.

Xiao, Y., Xu, T., and Pruess, K., 2009. The effects of gas-fluid-rock interactions on CO_2 injection and storage: insights from reactive transport modeling. *Energy Procedia*, 1 (1), 1783–1790. doi:10.1016/j.egypro.2009.01.233

Xu, T., Apps, J.A., and Pruess, K., 2003. Reactive geochemical transport simulation to study mineral trapping for CO_2 disposal in deep arenaceous formations. *Journal of Geophysical Research: Solid Earth*, 108 (B2). doi:10.1029/2002JB001979.

Xu, T., *et al.*, 2010. Reactive transport modeling to study changes in water chemistry induced by CO_2 injection at the Frio-I Brine Pilot. *Chemical Geology*, 271 (3–4), 153–164. doi:10.1016/j.chemgeo.2010.01.006

Yamamoto, S., *et al.*, 2013. Study on geomechanical stability of the aquifer -caprock system during CO_2 sequestration by coupled hydromechanical modelling. *Energy Procedia*, 37, 3989–3996. doi:10.1016/j.egypro.2013.06.298

Zhang, R., *et al.*, 2015. Sequentially coupled THMC model for CO2 geological sequestration into a 2D heterogeneous saline aquifer. *Journal of Natural Gas Science & Engineering*, 27, 579–615. doi:10.1016/j.jngse.2015.09.013

Zhang, R., *et al.*, 2012 A fully coupled model of nonisothermal multiphase flow, geomechanics, and chemistry during CO2 sequestration in brine aquifers. *Proceedings of the TOUGH Symposium*, Berkeley, California, 838–848.

Zhang, R., *et al.*, 2016. A fully coupled thermal-hydrological-mechanical-chemical model for CO_2 geological sequestration. *Journal of Natural Gas Science & Engineering*, 28, 280–304. doi:10.1016/j.jngse.2015.11.037

Zhou, X. and Burbey, T.J., 2014. Fluid effect on hydraulic fracture propagation behavior: a comparison between water and supercritical CO_2 -like fluid. *Geofluids*, 14 (2), 174–188. doi:10.1111/gfl.12061